Topology Optimization Using the Constrained Natural Element Method

Yanda Chen[*], Eric Monteiro[†], Imade Koutiri[‡] and Véronique Favier[§]
Arts et Metiers Institute of Technology, CNRS, CNAM, HESAM Universite, Paris, 75013, France

This paper focuses on a new topology optimization method for structures combining the solid isotropic material with penalization method (SIMP) and the constrained natural element method (CNEM). Common numerical instabilities such as checkerboard pattern and mesh dependency are studied and a new filter based on natural neighbors is proposed. Several 2D and 3D numerical examples are presented to demonstrate the effectiveness of the proposed method.

Nomenclature

$\boldsymbol{u}_I$	=	Nodal displacement vector
$\overline{\boldsymbol{\varepsilon}}_I$	=	Voronoi cell strain vector
$\boldsymbol{\sigma}_I$	=	Voronoi cell stress vector
$\overline{\boldsymbol{B}}_I$	=	Voronoi cell strain-displacement matrix
$\boldsymbol{C}$	=	Constitutive matrix
$\boldsymbol{K}$	=	Global stiffness matrix
$\boldsymbol{f}$	=	Global force vector
$\boldsymbol{\zeta}$	=	Adjoint vector
E	=	Young's modulus
v	=	Poisson's ratio
c	=	Compliance
V_I	=	Voronoi cell volume
ρ_I	=	Voronoi cell density
$\tilde{\rho}_I$	=	Voronoi cell physical density

I. Introduction

Topology optimization (TO) aims at determining the optimal material distribution in the design domain for a given set of boundary conditions. On one hand, the physical problems can be solved by numerical methods like finite element method (FEM) or meshless methods. On the other hand, the optimization can be completed by mathematical programming techniques such as the optimality criteria algorithm (OC) or the method of moving asymptotes (MMA). Several TO approaches have been proposed since the pioneer work by Bendsøe and Kikuchi in 1988[1], namely density-based method, level set-based method, homogenization method and evolutionary structural optimization method. The comparison and critical review of the above methods have been given in detail by Sigmund and Maute[2].

The FEM has been the most frequently used numerical method and its application based on density method in TO is very mature. However, FEM displays the checkerboard pathology and mesh dependency. The former consists in alternating void and solid elements while the latter shows lack of convergence to a specific topological layout with mesh refinement. To overcome these phenomena, several techniques have been proposed, such as the use of filters[3] or the substitution of FEM by polygonal finite element method[4] or meshless methods. For example,

---

Communicating Author: yanda.chen@ensam.eu

[*] Ph.D. student, laboratory PIMM, Arts et Metiers Institute of Technology, CNRS, CNAM, HESAM Universite, 151 Bd de l'Hôpital, 75013 Paris, France.

[†] Associate professor, laboratory PIMM, Arts et Metiers Institute of Technology, CNRS, CNAM, HESAM Universite, 151 Bd de l'Hôpital, 75013 Paris, France.

[‡] Associate professor, laboratory PIMM, Arts et Metiers Institute of Technology, CNRS, CNAM, HESAM Universite, 151 Bd de l'Hôpital, 75013 Paris, France.

[§] Full professor, laboratory PIMM, Arts et Metiers Institute of Technology, CNRS, CNAM, HESAM Universite, 151 Bd de l'Hôpital, 75013 Paris, France.

SIMP involving the Meshless Local Petrov-Galerkin (MLPG) mixed collocation method[5] has been applied to TO of elastic structures while Luo et al.[6] replaced MLPG by Element-free Galerkin Method (EFGM). Bi-directional evolutionary structural optimization (BESO) method combined with EFGM has also been proposed for TO by Shobeiri[7]. However, the major drawback of these meshless methods is the way to impose the essential boundary conditions since the interpolation functions do not satisfy the Kronecker delta property. Recently, an alternative employing the natural neighbor radial point interpolation method in tandem with BESO was suggested by Gonçalves et al[8].

In this paper, a new approach based on CNEM and SIMP is proposed to carry out TO of continuum structures. CNEM is a Galerkin method, based on the constrained Voronoi diagram of given nodes, that uses Laplace or Sibson interpolation. Unlike other common meshless techniques, the interpolation functions used in CNEM satisfy Kronecker delta property, which enable the imposition of essential boundary conditions as in FEM. Furthermore, thanks to the natural neighbor information established in the construction of interpolation functions, a new neighbor-based filter is proposed to avoid numerical instabilities.

II.   The Constrained Natural Element Method

Natural element method (NEM) is an efficient numerical method which was proposed by Braun and Sambridge[9] to solve partial differential equations with highly irregular meshes. Sukumar et al.[10] has shown that the interpolation between adjacent nodes in NEM along any convex boundary is strictly linear, which facilitates the application of essential boundary conditions. However, on non-convex boundaries, they may be affected by the nodes located within the domain or over the non-convex boundary far from the node under consideration. In order to solve this phenomenon, Cueto et al.[11] recovered the linearity of interpolation functions along any slightly non-convex boundary by invoking the concept of α-shape, which is called α-NEM. In order to accurately describe some geometric details, it is necessary to properly adjust the node density and the value of α. Moreover, the generalization of α-NEM in three-dimensional non-convex domains has not been proposed. In the case of strongly non-convex domains, Yvonnet et al.[12] put forward the CNEM, which introduced the visibility criteria in NEM to restrict the selection of natural neighbor relationship of node pairs to construct the interpolation functions and established the constrained Voronoi diagram in 2D. On this basis, Illoul and Lorong[13] extended its application to 3D. Once the constrained Voronoi diagram is constructed, the similar algorithm for constructing interpolation functions and calculating integration can be directly applied in CNEM as in NEM. At present, there is no research work exploring structural TO using NEM or CNEM.
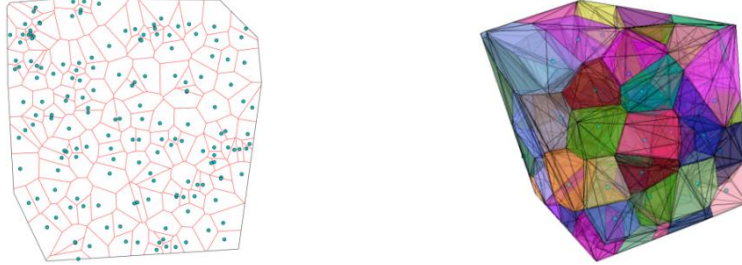
A. Constrained Voronoi Diagram

Figure 1. Voronoi diagram of a cloud of *N* nodes in 2D (left) and 3D (right)

In NEM, the Voronoi diagram of a cloud of N nodes, shown in Fig. 1, divides the bounded domain Ω^D in D-dimensions into a group of Voronoi cells $\mathcal{V}_I$, such that any point x within the Voronoi cell $\mathcal{V}_I$ is closer to node I than any other node J ($J{\neq}I$):

$$\mathcal{V}_I = \left\{ \boldsymbol{x} \in \Omega^D : \ d(\boldsymbol{x},\boldsymbol{x}_I) \leq d\left(\boldsymbol{x},\boldsymbol{x}_J\right) \forall J \neq I \right\} \tag{1}$$

where $\boldsymbol{x}_I$ represents the coordinates of node I and $d(\boldsymbol{x}_I,\boldsymbol{x}_J)$ the Euclidean distance between node I and node J. With this definition, if a segment connecting two neighbors crosses the domain boundary Γ, then node I influences node J, which is incorrect, see Fig. 2. To overcome this issue, a visibility criterion is introduced in the definition of Voronoi diagram to give rise to the constrained Voronoi diagram:

$$\mathcal{V}_I^C = \left\{ \boldsymbol{x} \in \Omega^D : \ d(\boldsymbol{x},\boldsymbol{x}_I) \leq d\left(\boldsymbol{x},\boldsymbol{x}_J\right) \forall J \neq I \ \cap \ x \ is \ visible \ from \ I \ and \ J \right\} \tag{2}$$
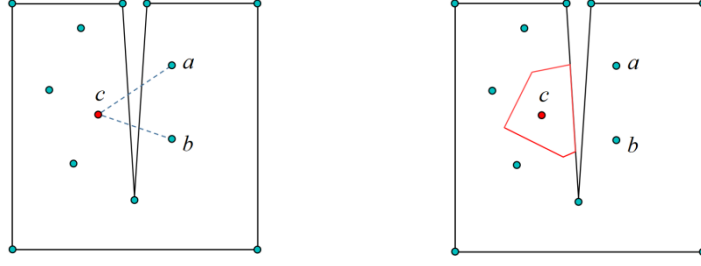
Figure 2. visibility criterion (left) and constrained Voronoi cell of node c (right)

B. Construction of interpolation functions

There exist different interpolation procedures that are based upon natural neighborhood. The Sibson interpolant[14] is one of the most widely used and its construction in 2D is shown in Fig. 3. First, the constrained Voronoi diagram of N nodes is modified locally by introducing a new Voronoi cell attached to point x (blue area). Then, the interpolation function is computed from geometrical considerations:

$$\phi_I^{Sib}(x) = \frac{L_I(x)}{L(x)} \quad with \quad L(x) = \sum_{J=1}^{n} L_J(x) \tag{3}$$

where $L_I(x)$ is the Lebesgue measure of the intersection (green area) of the initial Voronoi cell of node I (yellow area) and the new Voronoi cell of point x (blue area), $L(x)$ represents the Lebesgue measure of the new Voronoi cell of point x and n is the number of natural neighbors of point x. Unlike the FEM and other meshless methods, the construction of interpolation functions in CNEM is purely geometric, which does not involve user-defined parameters.
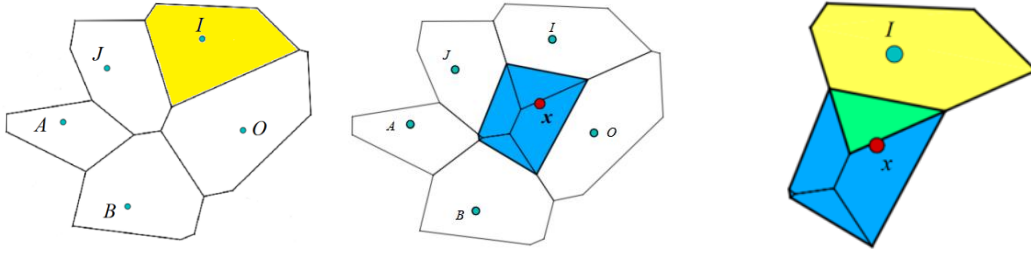

Figure 3. Process to compute Sibson interpolant in 2D

It has been proved that Sibson interpolant satisfies the Kronecker delta property, the partition of unity property and the linear consistency[10]:

$$\phi_I(x_J) = \delta_{IJ}, \quad \sum_{I=1}^{n} \phi_I(x) = 1, \quad u(x) = \sum_{I=1}^{n} \phi_I(x) u_I \tag{4}$$

C. CNEM discrete weak form

The governing equation of equilibrium of a linear elastic body Ω can be expressed as:

$$\nabla^T \sigma + b = 0 \tag{5}$$

subjected to the boundary conditions:

$$\sigma n = \bar{t} \tag{6}$$
$$u = \bar{u} \tag{7}$$

where σ and b are the stress tensor and body force vector respectively, $\bar{t}$ stands for the prescribed traction vector on the Von Neumann boundary Γ_t and $\bar{u}$ represents the prescribed displacement vector over the Dirichlet boundary Γ_u, n is the outer normal unit vector to the boundary $\Gamma = \Gamma_t \cup \Gamma_u$.

Introducing any arbitrary function δu, the associated weak form yields to:

$$\int_\Omega \delta\boldsymbol{\varepsilon}^T\boldsymbol{\sigma}d\Omega - \int_\Omega \delta\boldsymbol{u}^T\boldsymbol{b}d\Omega - \int_{\Gamma_d}\delta\boldsymbol{u}^T\boldsymbol{t}d\Gamma = 0 \tag{8}$$

In order to obtain the CNEM discrete weak form, the design domain Ω is represented by appropriately distributed nodes and the corresponding constrained Voronoi diagram. Then, using Eq. (3), the displacement at any point x can be expressed by:

$$\boldsymbol{u}^h(\boldsymbol{x}) = \sum_{I=1}^n \boldsymbol{\phi}_I(\boldsymbol{x})\boldsymbol{u}_I \tag{9}$$

where $\boldsymbol{\phi}_I$ and $\boldsymbol{u}_I$ are the interpolation function matrix and displacement vector of node I respectively. The strain vector $\boldsymbol{\varepsilon}$ at point x reads:

$$\boldsymbol{\varepsilon}(\boldsymbol{x}) = \boldsymbol{L}\boldsymbol{u}^h(\boldsymbol{x}) = \sum_{I=1}^n \boldsymbol{B}_I(\boldsymbol{x})\boldsymbol{u}_I \tag{10}$$

where $\boldsymbol{L}$ is the differential operator matrix and $\boldsymbol{B}_I$ represents the strain-displacement matrix of node I. Finally, using the constitutive equation, the stress vector can be obtained by:

$$\boldsymbol{\sigma}(\boldsymbol{x}) = \sum_{I=1}^n \boldsymbol{C}\boldsymbol{B}_I(\boldsymbol{x})\boldsymbol{u}_I \tag{11}$$

where $\boldsymbol{C}$ is the material constitutive matrix. For linear isotropic elastic materials in 2D under the assumption of plane strain, it can be defined as:

$$\boldsymbol{C} = \frac{E}{(1+v)(1-2v)}\begin{bmatrix} 1-v & v & 0 \\ v & 1-v & 0 \\ 0 & 0 & (1-2v)/2 \end{bmatrix} \tag{12}$$

where E and v are Young's modulus and poisson's ratio respectively.

Substituting Eqs. (9), (10) and (11) into Eq. (8), the discrete weak form reads:

$$\sum_{J=1}^N \sum_{I=1}^N \delta\boldsymbol{u}_J^T\left(\int_\Omega \boldsymbol{B}_J^T\boldsymbol{C}\boldsymbol{B}_I d\Omega\right)\boldsymbol{u}_I = \sum_{J=1}^N \delta\boldsymbol{u}_J^T\boldsymbol{f}_J \tag{13}$$

where N is the number of constrained Voronoi cells. Using the arbitrariness of $\boldsymbol{\delta u}$, Eq. (13) yields to the following matrix system:

$$\boldsymbol{Ku} = \boldsymbol{f} \tag{14}$$

where $\boldsymbol{K}$ is the global stiffness matrix and $\boldsymbol{f}$ the force vector.

The non-polynomial nature of CNEM interpolation functions leads to the use of a large number of Gauss integration points to accurately compute Eq.(13). To overcome this, the stabilized conforming nodal integration scheme (SCNI) proposed by Chen et al.[15] is applied in this study. Yvonnet et al.[12] showed that the SCNI scheme applied in 2D non-convex domains improve the efficiency and accuracy compared to standard gauss quadrature. In 3D case, Illoul and Lorong[13] found that SCNI has the same convergence speed as linear finite element based on Gaussian quadrature, but the total error is 1/3 of the latter. In SCNI, the strain smoothing stabilization is performed to stabilize the nodal integration:

$$\bar{\boldsymbol{\varepsilon}}_I(\boldsymbol{x}) = \frac{1}{L_I(x)}\int_{\Omega_I}\boldsymbol{B}_I(\boldsymbol{x})\boldsymbol{u}_I d\Omega \tag{15}$$

By applying the divergence theorem, Eq. (15) can be rewritten as:

$$\bar{\boldsymbol{\varepsilon}}_I(\boldsymbol{x}) = \frac{1}{L_I(x)}\oint_{\Gamma_I}\boldsymbol{\phi}_I(\boldsymbol{x})\boldsymbol{u}_I \cdot \boldsymbol{n}d\Gamma \tag{16}$$

III. Formulation of Topology Optimization Problem

The aim of TO is to obtain an optimized structure made of a mix of soft (void) and stiff (solid) materials. Density-based methods are the most popular TO approaches due to their simplicity and ease of implementation. In such approach, the design domain Ω^D is discretized and a design variable named density $\boldsymbol{\rho}$, is assigned to each

subdomain. Since discrete values usually lead to ill-conditioned problem, this density takes continuous values from 0 to 1. To limit intermediate values, the density can be penalized.

A. Problem Statement

The main objective of structural optimization problems is to minimize the deformation of structures constrained by volume. This can be achieved by minimizing strain energy stored in the structure, which is equivalent to minimizing compliance. The mathematical form of such a problem is written as:

$$
\begin{cases}
\min_{\boldsymbol{\rho} \in S} \; c(\boldsymbol{\rho}) = \boldsymbol{f}^T \boldsymbol{u}(\boldsymbol{\rho}) \\
s.t. \begin{cases}
\frac{\sum_{I=1}^N V_I \rho_I}{\overline{V}} - 1 \leq 0 \\
\boldsymbol{\rho}_{min} \leq \boldsymbol{\rho} \leq \boldsymbol{\rho}_{max} \\
\boldsymbol{f} = \boldsymbol{K}(\boldsymbol{\rho})\boldsymbol{u}(\boldsymbol{\rho})
\end{cases}
\end{cases}
\tag{17}
$$

where $\overline{V}$ is the overall volume constraint, c is the compliance value, $\boldsymbol{\rho}_{min}$ and $\boldsymbol{\rho}_{max}$ are the lower and upper bounds of the design variables, $\boldsymbol{f} = \boldsymbol{Ku}$ is the equilibrium equation from Eq. (14).

In the modified SIMP, it is necessary to artificially set the functional relationship between the density of constrained Voronoi cells and the physical properties of material. Considering linear isotropic materials, the Young's modulus can be calculated as:

$$
E(\boldsymbol{\rho}) = [\epsilon + (1 - \epsilon)\boldsymbol{\rho}^p]E_0
\tag{18}
$$

where E_0 is the Young's modulus for $\rho = 1$, ϵ is a small value to prevent singularity, e.g. $\epsilon = 10^{-4}$, p is a penalty factor whose value is 3.5 in this paper.

B. Filter Operator

Filter operator is one of the techniques to avoid numerical instabilities in TO. The commonly used parameter of the density filter, the weight factor, is defined as:

$$
H_J^{dens} = max\langle 0, R - d(\boldsymbol{x}_J, \boldsymbol{x}_I)\rangle
\tag{19}
$$

where R is the radius of the filter. All nodes whose distance to the current node is lower than radius R will contribute. Fig. 4 (left) shows an example in 2D where the radius defines a circular neighborhood. For 3D problems, the filtering area forms a sphere. The filtered density of node I is determined by the following formula:

$$
\tilde{\rho}_I = \left(\sum_{J=1}^{n_f} H_J \rho_J\right) / \left(\sum_{J=1}^{n_f} H_J\right)
\tag{20}
$$

where n_f is the number of nodes within the filtering domain.

The disadvantage of the density filter is that when the design domain or the distribution of nodes is irregular, the filtering effect may be poor, because there are not enough nodes captured within filtering domains or the results are biased to the side where the nodes are more densely distributed. For example, the density of node I in Fig. 4 (left) is mainly contributed by the nodes on the left and the bottom, while the node on the right side does not even contribute to it.

In this paper, a new filter, based on natural neighbors and shown in Fig. 4 (right), is proposed. This filter can more reasonably consider the contribution of the neighbor nodes in all directions under irregular conditions, and the only parameter that needs to be defined is the number of layers. The weight factor for neighbor-based filter of node I is expressed as:

$$
H_J^{neig} = \begin{cases} d_{max} - d(\boldsymbol{x}_J, \boldsymbol{x}_I) & if\ J\ is\ a\ neighbor \\ 0 & else \end{cases}
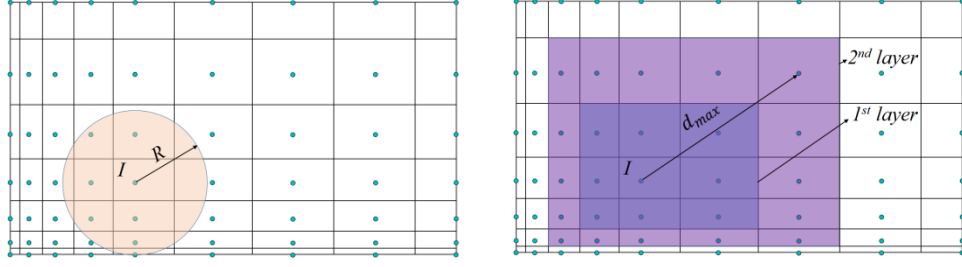\tag{21}
$$

Figure 4. standard density filter (left) and neighbor-based filter (right)

where d_{max} represents the maximum distance between the target node and the neighbor node within the filtering domain. Then, the filtered density can be calculated by Eq. (20).

C. Sensitivity analysis

Sensitivity analysis is an effective method to determine whether and how much the density of a specific constrained Voronoi cell should be increased or decreased. The adjoint method is adopted here to calculate the gradient information of design variables. Thus, the objective function is modified by adding a zero part from the equilibrium equation:

$$c(\tilde{\rho}) = f^T u(\tilde{\rho}) + \zeta^T (K(\tilde{\rho})u(\tilde{\rho}) - f) \tag{22}$$

where ζ is an adjoint vector which can take arbitrary values. Then the partial derivative of the objective function c to design variable ρ_I of constrained Voronoi cell I can be obtained as:

$$\frac{\partial c(\tilde{\rho})}{\partial \rho_I} = \left[\zeta^T \frac{\partial K(\tilde{\rho})}{\partial \tilde{\rho}_I} u(\tilde{\rho}) + \left(f^T + \zeta^T K(\tilde{\rho}) \right) \frac{\partial u(\tilde{\rho})}{\partial \tilde{\rho}_I} \right] \frac{\partial \tilde{\rho}_I}{\partial \rho_I} \tag{23}$$

In order to get rid of the derivation of the displacement to the design variable, it is necessary that the term in brackets (adjoint equation) is equal to zero, which means:

$$\zeta^T = f^T K(\tilde{\rho})^{-1} = -u(\tilde{\rho})^T \tag{24}$$

Thus, the derivative of the objective function becomes:

$$\frac{\partial c(\tilde{\rho})}{\partial \rho_I} = \left(\zeta^T \frac{\partial K(\tilde{\rho})}{\partial \tilde{\rho}_I} u(\tilde{\rho}) \right) \frac{\partial \tilde{\rho}_I}{\partial \rho_I} \tag{25}$$

Based on the SIMP form in Eq. (18), Eq. (25) can be expressed in the following discrete form:

$$\frac{\partial c(\tilde{\rho})}{\partial \rho_I} = \left[\zeta^T \overline{B}_I^T \left((1 - \epsilon) p \tilde{\rho}_I^{p-1} L(x_I) \right) C \overline{B}_I u(\tilde{\rho}) \right] \frac{\partial \tilde{\rho}_I}{\partial \rho_I} \tag{26}$$

The gradient of the constraint function V_I to design variable ρ_I of constrained Voronoi cell I is:

$$\frac{\partial V_I(\tilde{\rho})}{\partial \rho_I} = V_I \frac{\partial \tilde{\rho}_I}{\partial \rho_I} \tag{27}$$

where $\partial \tilde{\rho}_I / \partial \rho_I = H_J / (\sum_{J=1}^{n_f} H_J)$ in all the above formulas.

D. Optimizers

The performance of topology optimization in terms of convergence and efficiency is highly dependent on the choice of the optimizer. The optimization problem expressed in Eq. (17) can be solved by OC, MMA or its globally convergent version GCMMA. The application of each needs the first derivative information of the objective function and of the constraint to design variables. In order to compare the influence of different optimizers on the results, the above three optimizers are all implemented in this study. For the selection of the parameters in OC, MMA or GCMMA, we refer to Andreassen et al.[19] and Liu et al.[20] respectively.

In this research, the update scheme for the density in OC can be expressed by[16]:

$$\rho_I^{k+1} \begin{cases} max(\rho_{min}, \rho_I^k - m) & \rho_I^k B_I^\eta \leq max(\rho_{min}, \rho_I^k - m) \\ \rho_I^k B_I^\eta & max(\rho_{min}, \rho_I^k - m) < \rho_I^k B_I^\eta < min(\rho_{max}, \rho_I^k + m) \\ min(\rho_{max}, \rho_I^k + m) & min(\rho_{max}, \rho_I^k + m) \leq \rho_I^k B_I^\eta \end{cases} \tag{28}$$

where k indicates the current iteration number, m is the positive moving limit, η is a numerical damping coefficient which is used to ensure the stability of the convergence, B_I is derived from the optimality condition and can be expressed as follows:

$$B_I^k = -\frac{\partial c(\tilde{\rho})}{\partial \rho_I} \left(\lambda \frac{\partial L(\tilde{\rho}_I)}{\partial \rho_I} \right)^{-1} \tag{29}$$

where λ is a Lagrange multiplier which can be determined by a bi-sectioning algorithm[16].

The MMA approach proposed by Svanberg[18] is based on the first order Taylor expansion of the objective and constraint functions, in which a general form of the TO problem can be rewritten as:

$$\begin{cases} min\, f_0(\tilde{\boldsymbol{\rho}}) + a_0 z + \sum_{j=1}^m \left(c_j y_j + \frac{1}{2} d_j y_j^2 \right) \\ s.t. \begin{cases} f_j(\tilde{\boldsymbol{\rho}}) - a_j z - y_j \leq 0 & j = 1,\ldots,m \\ y_j \geq 0 & j = 1,\ldots,m \\ z \geq 0 \\ \boldsymbol{\rho}_{min} \leq \boldsymbol{\rho} \leq \boldsymbol{\rho}_{max} \\ \boldsymbol{f} = \boldsymbol{K}(\tilde{\boldsymbol{\rho}})\boldsymbol{u}(\tilde{\boldsymbol{\rho}}) \end{cases} \end{cases} \tag{30}$$

where a_0, a_j, c_j, and d_j are positive real numbers, $\boldsymbol{y}$ and z are artificially added design variables.

In MMA, the objective and constraint functions are linearly expanded to construct a convex sub-problem, then, the sub-problem is solved to approximate the initial problem. The sub-problem can be expressed as:

$$\begin{cases} min\, \overline{f}_0^{(k)}(\tilde{\boldsymbol{\rho}}) + a_0 z + \sum_{j=1}^m \left(c_j y_j + \frac{1}{2} d_j y_j^2 \right) \\ s.t. \begin{cases} \overline{f}_j^{(k)}(\tilde{\boldsymbol{\rho}}) - a_j z - y_j \leq 0 & j = 1,\ldots,m \\ y_j \geq 0 & j = 1,\ldots,m \\ z \geq 0 \\ \boldsymbol{\rho}_{min} \leq \boldsymbol{\rho} \leq \boldsymbol{\rho}_{max} \\ \boldsymbol{f} = \boldsymbol{K}(\tilde{\boldsymbol{\rho}})\boldsymbol{u}(\tilde{\boldsymbol{\rho}}) \end{cases} \end{cases} \tag{31}$$

where

$$\overline{f}_j^{(k)}(\tilde{\boldsymbol{\rho}}) = f_j(\tilde{\boldsymbol{\rho}}^{(k)}) + \sum_{i=1}^n \left(\frac{P_{ij}^{(k)}}{U_i^{(k)} - \tilde{\rho}_j} + \frac{Q_{ij}^{(k)}}{\tilde{\rho}_i - L_i^{(k)}} \right) \tag{32}$$

The generation of the convex sub-problems are not only based on the gradient information of the current iteration point (contained in P_{ij} and Q_{ij}), but also based on the moving asymptotes L_i and U_i, which are updated in each iteration based on the information from the previous iteration point.
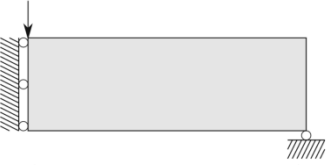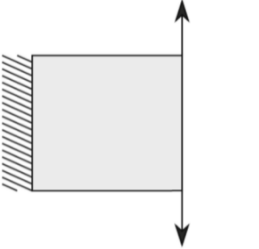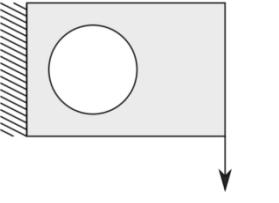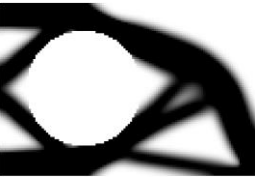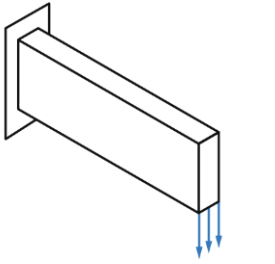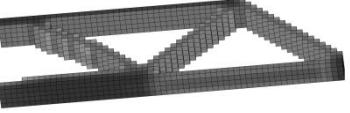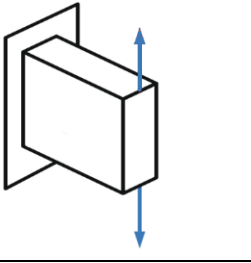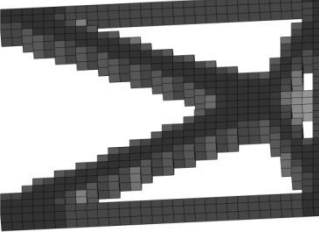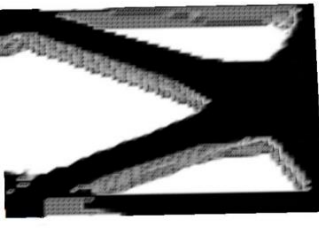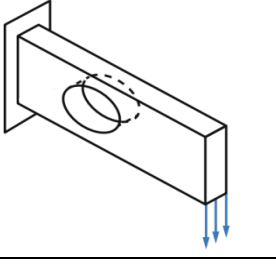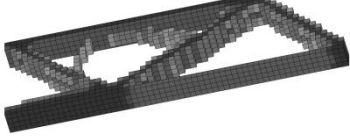
The GCMMA differs from MMA in that it attempts to achieve global convergence by controlling a non-monotonous parameter (which is a fixed small value in MMA) and invokes the internal iterations in the convex approximation. The construction of convex sub-problem and the update schemes of parameters have been given in detail by Svanberg[18,19]. Finally, the sub-problems in MMA and GCMMA are solved by using a primal-dual interior point algorithm[18,19].

The convergence criteria considered in this study is the absolute value of the maximum density change in two continuous topologies. Based on this definition, the convergence criteria is defined as:

$$max|\boldsymbol{\rho}^{k+1} - \boldsymbol{\rho}^k| \leq \delta \tag{33}$$

where δ is the allowable tolerance.

Table 1. Topology optimization results for 2D and 3D structures

TO case	FEM result[17,20]	CNEM result
1		
2		
3		
4		
5		
6		

IV.   Numerical Examples

In this section, several 2D and 3D examples are presented to illustrate the effectiveness of the proposed method. Results are listed in Table 1. All tests are considered dimensionless: $E_0 = 1$, $v = 0.3$, and $f = 1$. The optimization algorithm adopted here is OC and the plane strain assumption is made in 2D cases. The number of neighbor-based filter layer is 3. The optimized results obtained by FEM using density filter in references[17,22] are also listed in the second column for comparison. Good agreement is observed in all cases.

The optimized results obtained using three different optimizers for a cantilever beam are shown in Table 2 and the corresponding evolution history of the objective function over the first 50 iterations is shown in Fig. 5. In this study, the length and width of cantilever beam are 120 and 40 respectively. In these calculations, the same moving limit $m = 0.5$ is adopted for all optimizers. It can be seen that OC method is able to achieve faster convergence at the beginning, but the final objective function value is also the largest. The iterative process of MMA is close to GCMMA, and their final objective function values are slightly smaller than that of OC. We also compare the optimized results in Table 2 quantitatively by measuring three angles of the optimized results. The results obtained by OC and GCMMA are consistent, the third angle in MMA is slightly larger than the other two, as shown in Fig. 6.

In order to further verify the mesh insensitivity of our proposed method, we select two discretization schemes, regular and irregular, respectively. Each scheme uses four different number of Voronoi cells in turn: 2821, 3434, 4107 and 4961. Similarly, using the three angles in Fig. 6 as the benchmark, the comparison results of eight different discretization schemes is shown in Fig. 7. It can be seen that the histogram of each angle is relatively stable, and the fluctuation does not exceed 4 degrees. These results prove that the method proposed in this paper is not affected by the discretization scheme.

Finally, the effect of different filters on the optimized results when the discretization is highly irregular is shown in Fig. 8 and Fig. 9, where s is the length of the structure. When the design domain and the discretization scheme are both regular or slightly irregular, the numerical instabilities can be avoided by using the density filter as well as the neighbors-based filter. However, when the situation becomes highly irregular, the numerical instabilities may still exist if the radius used in the density filter is too small, as shown in Fig. 8. This means that the filter radius which performs well in regular discretization may not be applicable in irregular case. Furthermore, the relationship between filter radius and design domain size and discretization scheme is usually determined by trial and error or experience since there is no established relationship between them. Fig. 9 shows the optimized results by neighbor-based filter with different number of layers for the same discretization. There are no numerical instabilities even when the number of filter layer is equal to 1.

V.   Conclusion

In this paper, an effective method for TO of structures is developed by combining CNEM with SIMP. In CNEM, the Sibson interpolation and SCNI are used to improve the stability and accuracy. A new neighbor-based filter is also proposed to face highly irregular discretization. Numerical examples in 2D and 3D involving different optimizers and discretization schemes (regular and irregular) have shown the robustness of the method.
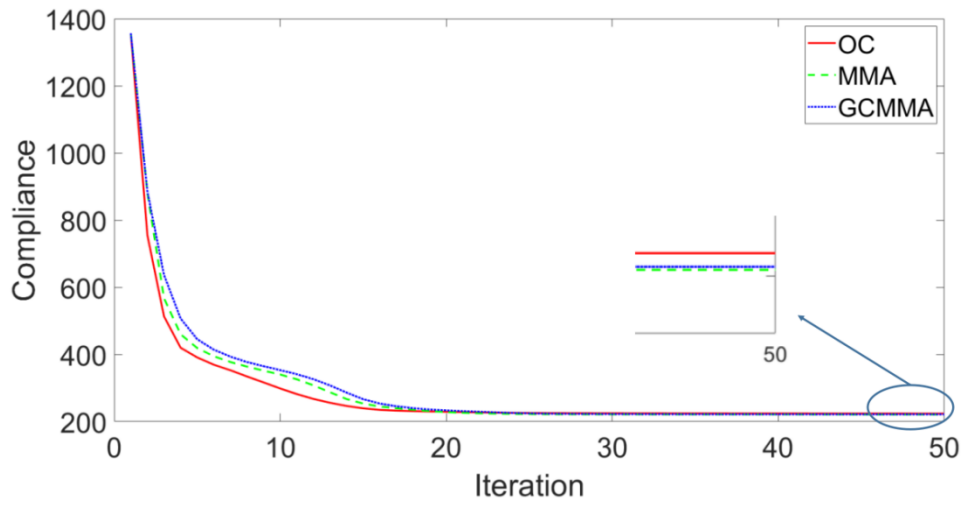
Figure 5. Evolution history of the objective function over iterations with different optimizers
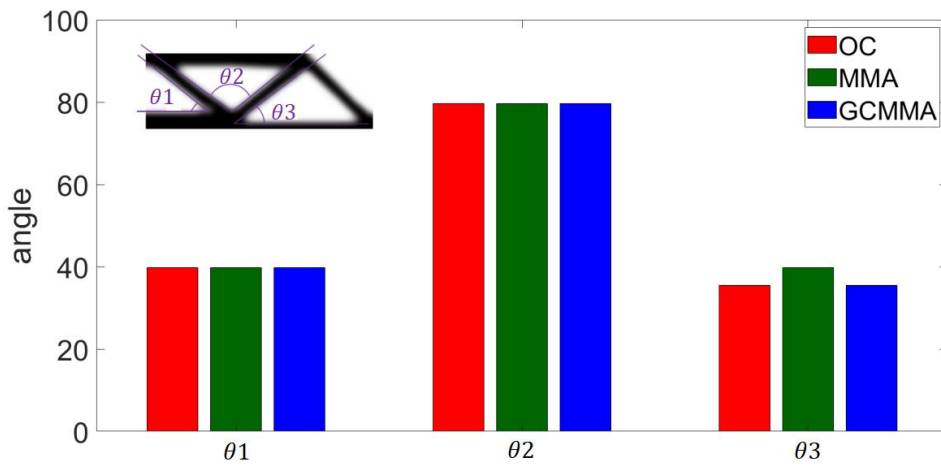

Figure 6. Comparison of angles in optimized results obtained by different optimizers

Table 2. Topology optimization results with OC, MMA and GCMMA

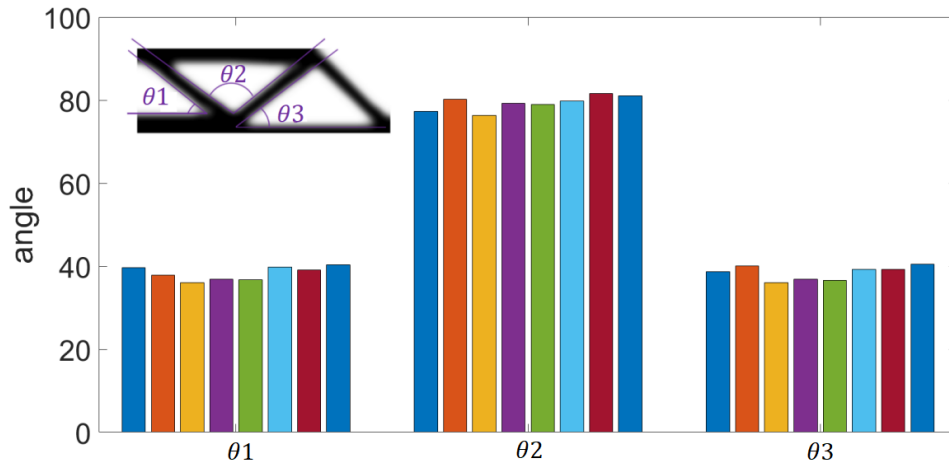| optimizer	OC	MMA	GCMMA
CNEM result			

Figure 7. Comparison of angles in optimized results obtained by different discretization

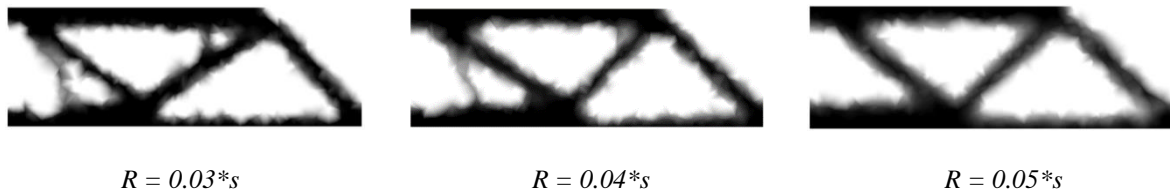*R = 0.03*s*   *R = 0.04*s*   *R = 0.05*s*

Figure 8. Optimized results using density filter for different filter radius

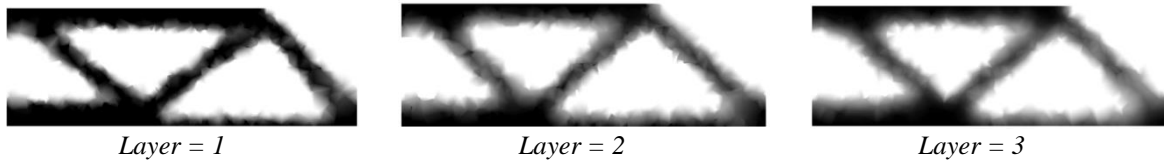*Layer = 1*   *Layer = 2*   *Layer = 3*

Figure 9. Optimized results using neighbor-based filter for different filter layers

References

[1]Bendsøe, M.P., and Kikuchi. N., "Generating optimal topologies in structural design using a homogenization method," Computer Methods in Applied Mechanics and Engineering, Vol. 71, NO. 2, 1988, pp. 197-224.

[2]Sigmund, O., and Maute. K., "Topology optimization approaches," Structural and Multidisciplinary Optimization, Vol. 48, 2013, pp. 1031-1055.

[3]Sigmund. O., "Morphology-based black and white filters for topology optimization," Structural and Multidisciplinary Optimization, Vol. 33, 2007, pp. 401–424.

[4]Talischi, C., and Paulino. G.H., "Addressing integration error for polygonal finite elements through polynomial projections: A patch test connection," Mathematical Models and Methods in Applied Sciences, Vol. 24, NO. 8, 2014, pp. 1701-1727.

[5]Shu, L., and Atluri. S.N., "Topology-optimization of structures based on the MLPG mixed collocation method," Computer Modeling in Engineering & Sciences, Vol. 26, NO. 1, 2008, pp. 61-74.

[6]Zhen, L., Nong, Z., Yu, W., and Wei, G., "Topology optimization of structures using meshless density variable approximants," International Journal for Numerical Methods in Engineering, Vol. 93, NO. 4, 2013, pp. 443-464.

[7]Shobeiri. V., "Topology optimization using bi-directional evolutionary structural optimization based on the element-free Galerkin method," Vol. 48, NO. 3, 2015, pp. 380-396.

[8]Gonçalvesa, D.C., Lopesb, J.D.F., Campilhob, R.D.S.G., and Belinha, J., "Topology optimization using a natural neighbour meshless method combined with a bi-directional evolutionary algorithm," Mathematics and Computers in Simulation, Vol. 194, 2022, pp. 308–328.

[9]Braun, J., and Sambridge, M., "A numerical method for solving partial differential equations on highly irregular evolving grids," Nature, Vol. 376, 1995, pp. 655–660.

[10]Sukumar, N., Moran, B., and T. Belytschko., "The natural element method in solid mechanics," International Journal for Numerical Methods in Engineering, Vol. 43, 1998, pp. 839–887.

[11]Cueto, E., Doblaré, M., and Gracia, L., "Imposing essential boundary conditions in the natural element method by means of density-scaled α-shapes," International Journal for Numerical Methods in Engineering, Vol. 49, NO. 4, 2000, pp. 519-546.

[12]Yvonnet, J., Ryckelynck, D., Lorong, P., and Chinesta. F., "A new extension of the natural element method for non-convex and discontnuous problems: the constrained natural element method," International Journal for Numerical Methods in Enginering, Vol. 60, 2004, pp.1451-1474.

[13]Illoul, L., and Lorong. P., "On some aspects of the CNEM implementation in 3D in order to simulate high speed machining or shearing," Computers and Structures, Vol. 89, No. 11-12, 2011, pp. 940-958.

[14]Sibson, R., "A brief description of natural neighbor interpolation," Interpreting Multivariate Data, John Wiley & Sons, New York, 1981, pp. 21-36.

[15]Chen, J.S., Wu, C.T., Yoon, S., and You, Y., "A stabilized conforming nodal integration for Galerkin mesh-free methods," International Journal for Numerical Methods in Engineering, Vol. 50, 2001, pp. 435-466.

[16]Sigmund. O., "A 99 line topology optimization code written in Matlab," Structural and Multidisciplinary Optimization, Vol. 21,2001, pp. 120–127.

[17]Andreassen, E., Clausen, A., Schevenels, M., Lazarov, B.S., and Sigmund, O., "Efficient topology optimization in MATLAB using 88 lines of code," Structural and Multidisciplinary Optimization, Vol. 43, 2011, pp. 1–16.

[18]Svanberg, K., "The method of moving asymptotes - a new method for structural optimization," International Journal for Numerical Methods in Engineering, Vol. 24, 1987, pp. 359-373.

[19]Svanberg, K., "MMA and GCMMA–two methods for nonlinear optimization," vol. 1, 2007, pp. 1–15. URL: https://people.kth.se/~krille/mmagcmma.pdf.

[20]Liu, K., and Tovar, A., "An efficient 3D topology optimization code written in Matlab," Structural and Multidisciplinary Optimization, Vol. 50, 2014, pp. 1175–1196.